

## CONSTRAINING EMISSION MODELS OF LUMINOUS BLAZAR SOURCES

MAREK SIKORA<sup>1</sup>, ŁUKASZ STAWARZ<sup>2,3,4</sup>, RAFAŁ MODERSKI<sup>1</sup>, KRZYSZTOF NALEWAJKO<sup>1</sup>, AND GREG M. MADEJSKI<sup>2,4</sup>

<sup>1</sup> Nicolaus Copernicus Astronomical Center, Bartycka 18, 00-716 Warsaw, Poland; sikora@camk.edu.pl

<sup>2</sup> Kavli Institute for Particle Astrophysics and Cosmology, Stanford University, Stanford, CA 94305, USA

<sup>3</sup> Astronomical Observatory, Jagiellonian University, ul. Orła 171, 30-244 Kraków, Poland

<sup>4</sup> Stanford Linear Accelerator Center, 2575 Sand Hill Road, Menlo Park, CA 94025, USA

Received 2009 April 7; accepted 2009 August 21; published 2009 September 18

### ABSTRACT

Many luminous blazars which are associated with quasar-type active galactic nuclei display broadband spectra characterized by a large luminosity ratio of their high-energy ( $\gamma$ -ray) and low-energy (synchrotron) spectral components. This large ratio, reaching values up to 100, challenges the standard synchrotron self-Compton models by means of substantial departures from the minimum power condition. Luminous blazars also typically have very hard X-ray spectra, and those in turn seem to challenge hadronic scenarios for the high-energy blazar emission. As shown in this paper, no such problems are faced by the models which involve Comptonization of radiation provided by a broad-line region, or dusty molecular torus. The lack or weakness of bulk-Compton and Klein–Nishina features indicated by the presently available data favors the production of  $\gamma$ -rays via upscattering of infrared photons from hot dust. This implies that the blazar emission zone is located at parsec-scale distances from the nucleus, and as such is possibly associated with the extended, quasi-stationary reconfinement shocks formed in relativistic outflows. This scenario predicts characteristic timescales for flux changes in luminous blazars to be days/weeks, consistent with the variability patterns observed in such systems at infrared, optical, and  $\gamma$ -ray frequencies. We also propose that the parsec-scale blazar activity can be occasionally accompanied by dissipative events taking place at sub-parsec distances and powered by internal shocks and/or reconnection of magnetic fields. These could account for the multiwavelength intraday flares occasionally observed in powerful blazar sources.

*Key words:* acceleration of particles – galaxies: active – galaxies: jets – gamma rays: theory – quasars: general – radiation mechanisms: non-thermal

### 1. INTRODUCTION

Blazars are active galactic nuclei (AGNs) dominated by Doppler boosted radiation of relativistic jets, and as such, they provide an exceptional opportunity for studying the physics of innermost portions of AGN jets. However, in order to take advantage of this opportunity, the appropriate radiative processes responsible for generation of a broadband jet emission must be identified. And, while the low-energy component of double-peaked blazar spectra is uniquely identified as originating via the synchrotron radiation of ultrarelativistic electrons (hereafter by electrons we mean both electrons and positrons), the origin of the high-energy spectral component is still under debate. Possible contributions include inverse-Compton (IC) emission by electrons directly accelerated within the jet (and producing the observed synchrotron continuum), synchrotron radiation of pair cascades powered by hadronic processes, and synchrotron emission of ultra-high-energy protons and muons (see reviews by Sikora & Madejski 2001; Levinson 2006; Böttcher 2007). Seed photons for the IC process may be provided by the jet synchrotron emission as well as by the external photon sources, such as an accretion disk, broad-line regions (BLR) and/or dusty tori (hereafter “hot dust region,” HDR). The IC models involving Comptonization of local synchrotron radiation are called synchrotron-self-Compton (SSC) models, and those involving Comptonization of external radiation—external-radiation-Compton, or, for short, external-Compton (EC) models.

In this paper, we focus on blazars with a dense radiative circumnuclear environment, i.e., those hosted by quasars. High-energy (HE;  $\gamma$ -ray) luminosities of many of those objects exceed their low-energy (LE; synchrotron) luminosities by a factor  $q \equiv L_{\text{HE}}/L_{\text{LE}} = 10\text{--}100$ . At the same time, their X-ray spectra are often very hard, in a number of cases characterized by energy

spectral indices  $\alpha_x < 0.5$  (see Table 1 and references therein). Constraints resulting from such properties are discussed in Section 2 and Section 3, respectively. In addition, we investigate constraints imposed by the spectral localization of the two prominent blazar radiative components (Section 4), by the lack of theoretically predicted bulk-Compton features in blazar spectra (Section 5), and by the lack of signatures of the Klein–Nishina (KN) features in their synchrotron continua (Section 6). We discuss EC(BLR) and EC(HDR) models in Section 7, highlighting their similarities and differences. We discuss the possibility of detecting electromagnetic imprints of the presence of protons in the blazar jet spectra in Section 8. Our final results regarding physics of the parsec-scale jets of quasars are presented in Section 9, and we briefly conclude in Section 10. Throughout the paper, the approximation  $\theta_j = \theta_{\text{obs}} = 1/\Gamma$  is used, where  $\theta_j$  is the opening angle of a conical jet,  $\theta_{\text{obs}}$  is the angle between the line of sight and the jet axis, and  $\Gamma$  is the jet Lorentz factor. We also neglect the redshift dependence in the derived expressions, but note that this dependence goes at most as a factor  $(1+z)$ .

### 2. LARGE LUMINOSITY RATIO

Since our understanding of particle acceleration processes in a relativistic plasma is limited (and relies primarily on results obtained strictly in the test-particle limit), the existing hadronic models are not sufficiently quantitative to make robust predictions regarding the relative power required to be injected in the form of high-energy protons and ultrarelativistic electrons. Hence, the observed large luminosity ratio between the high- and the low-energy components in blazar spectra can be scaled by a free parameter in those models. In contrast, in leptonic scenarios both components are produced by the same population of

ultrarelativistic electrons, and therefore the observed large values of  $q$  provide valuable constraints on the blazar parameters.

Noting that for luminous, quasar-associated blazars, the KN and the pair production effects are likely to be insignificant (Moderski et al. 2005; see also Section 6), and that the effect of the anisotropy of EC scattering in the source comoving frame is negligible for  $\theta_{\text{obs}} \sim 1/\Gamma$  (Dermer 1995; Moderski et al. 2003), the following ratios of energy densities can be approximated as being equal:

$$\frac{u'_{\text{SSC}}}{u'_{\text{syn}}} \simeq \frac{u'_{\text{syn}}}{u'_B} \simeq \frac{u'_{\text{EC}}}{u'_{\text{ext}}} \equiv A, \quad (1)$$

where  $A$  is the ‘‘Thomson amplification factor,’’  $u'_B$  is the comoving magnetic energy density, while  $u'_{\text{syn}}$ ,  $u'_{\text{SSC}}$ ,  $u'_{\text{ext}}$  and  $u'_{\text{EC}}$  are the energy densities of the synchrotron, SSC, external (BLR or HDR), and EC photon fields, respectively, all as measured in the source rest frame.

### 2.1. Large Luminosity Ratio in the SSC Model

In the case of the SSC emission dominating the high-energy spectral component,  $L_{\text{HE}} \simeq L_{\text{SSC}}$ , one has

$$q \simeq \frac{L_{\text{SSC}}}{L_{\text{syn}}} \simeq \frac{u'_{\text{SSC}}}{u'_{\text{syn}}} \simeq \frac{u'_{\text{syn}}}{u'_B} = A \quad (2)$$

and

$$\frac{u'_B}{u'_{\text{SSC}}} \simeq \frac{u'_B}{u'_{\text{syn}}} \frac{u'_{\text{syn}}}{u'_{\text{SSC}}} = A^{-2} = q^{-2}, \quad (3)$$

where  $L_{\text{syn}}$  and  $L_{\text{SSC}}$  are the observed synchrotron and SSC luminosities, respectively. Noting next that the approximate relation between the ratio of total energy densities stored in non-thermal photons,  $u'_{\text{rad}}$ , and electrons,  $u'_e$ , is

$$\frac{u'_{\text{rad}}}{u'_e} \simeq \frac{\eta_{\text{rad}}}{1 - \eta_{\text{rad}}}, \quad (4)$$

where  $\eta_{\text{rad}}$  is the radiative efficiency of the injected electrons, and that in the SSC model with  $q \gg 1$  one has  $u'_{\text{rad}} \simeq u'_{\text{SSC}}$ , we obtain

$$\frac{u'_B}{u'_e} \simeq \frac{u'_B}{u'_{\text{SSC}}} \frac{u'_{\text{SSC}}}{u'_e} \simeq \frac{1}{q^2} \frac{\eta_{\text{rad}}}{(1 - \eta_{\text{rad}})}. \quad (5)$$

Since for the luminous blazars  $\eta_{\text{rad}} > 0.5$ , the ‘‘high- $q$  states’’ of the SSC-dominated  $\gamma$ -ray emission can be reached only for  $u'_e/u'_B > q^2 \gg 1$ , i.e., for conditions far away from equipartition.

### 2.2. Large Luminosity Ratio in the EC Models

In the case of the high-energy emission dominated by the EC radiation, we have  $L_{\text{HE}} \simeq L_{\text{EC}}$ , leading to

$$q = \frac{L_{\text{EC}}}{L_{\text{syn}}} \simeq \frac{u'_{\text{EC}}}{u'_{\text{syn}}} \simeq \frac{u'_{\text{ext}}}{u'_B} \quad (6)$$

and

$$\frac{u'_B}{u'_{\text{EC}}} \simeq \frac{u'_B}{u'_{\text{syn}}} \frac{u'_{\text{syn}}}{u'_{\text{EC}}} = A^{-1} q^{-1}. \quad (7)$$

Hence, with the further approximation  $u'_{\text{rad}} \simeq u'_{\text{EC}}$  (as justified for  $q \gg 1$ ), we obtain

$$\frac{u'_B}{u'_e} \simeq \frac{u'_B}{u'_{\text{EC}}} \frac{u'_{\text{EC}}}{u'_e} \simeq \frac{1}{Aq} \frac{\eta_{\text{rad}}}{(1 - \eta_{\text{rad}})}. \quad (8)$$

Obviously, in the EC models the quantities  $A$  and  $q$  are not equivalent, and the equipartition between the magnetic field and electron energy densities can be reached for any (large) value of the  $q$  parameter provided

$$A = \frac{1}{q} \frac{\eta_{\text{rad}}}{(1 - \eta_{\text{rad}})}. \quad (9)$$

Moreover, since  $A \simeq u'_{\text{EC}}/u'_{\text{ext}}$ , where

$$u'_{\text{EC}} \simeq \frac{L_{\text{EC}}}{4\pi R^2 c \Gamma^4} \quad (10)$$

and

$$u'_{\text{ext}} \simeq \frac{\Gamma^2 \xi_{\text{ext}} L_{\text{disk}}}{4\pi r^2 c}, \quad (11)$$

one may find that

$$A = \frac{L_{\text{EC}}}{\xi_{\text{ext}} L_{\text{disk}} \Gamma^4}. \quad (12)$$

In the above, we have introduced the distance of a blazar emission zone from the nucleus  $r$ , the radius of the emission zone  $R \simeq r \theta_j \simeq r/\Gamma$ , the accretion disk luminosity  $L_{\text{disk}}$ , and the fraction  $\xi_{\text{ext}}$  of the disk radiation reprocessed in the BLR or HDR. This, when combined with Equation (8), shows that the minimum power condition  $u'_B \sim u'_e$  implies bulk Lorentz factors of the emitting plasma:

$$\Gamma \simeq 20 \times \left[ \left( \frac{q}{10} \right) \left( \frac{\xi_{\text{ext}}}{0.1} \right)^{-1} \left( \frac{L_{\text{EC}}}{10^{49} \text{ erg s}^{-1}} \right) \times \left( \frac{L_{\text{disk}}}{10^{46} \text{ erg s}^{-1}} \right)^{-1} \left( \frac{1 - \eta_{\text{rad}}}{\eta_{\text{rad}}} \right) \right]^{1/4}. \quad (13)$$

We note that typically in blazar sources the disk luminosity  $L_{\text{disk}}$  cannot be observed directly but instead can be estimated from the observed luminosity of broad emission lines, leading to  $L_{\text{disk}} \gtrsim 10^{46} \text{ erg s}^{-1}$ . Also, the derived ‘‘equipartition’’ value of the jet Lorentz factor, which depends only weakly on the model parameters, is nicely consistent with the typical values implied by the observed superluminal expansion of pc/kpc-scale radio blobs in  $\gamma$ -ray bright, quasar-hosted blazars (Jorstad et al. 2001a, 2001b; Lister et al. 2009; Kovalev et al. 2009).

## 3. HARD X-RAY SPECTRA

About 30% of blazars detected by BeppoSAX up to an energy of 50 keV are characterized by very hard X-ray spectra, with the X-ray spectral indices smaller than the ‘‘canonical’’ value 0.5 (Giommi et al. 2002; Donato et al. 2005; see also Table 1). In several cases, strong indications were found for such hard spectra to extend up to at least  $\sim 100$  keV. Such hard spectra must be produced in a slow-cooling regime for the radiating particles, and below we investigate what constraints such observations impose on different emission models.

### 3.1. Hard X-ray Spectra in the Hadronic Models

#### 3.1.1. Proton-Initiated Cascades

In the hadronic models for luminous blazars, the observed X-ray emission is produced by synchrotron radiation of pair cascades powered by ultrarelativistic protons (Mannheim & Biermann 1992; Mannheim 1993). In order to obtain  $\alpha_x < 0.5$ ,

**Table 1**  
Luminous Blazar Sources with the Hardest Recorded X-ray Spectra

Name (1)	$z$ (2)	$\alpha_x$ (3)	$\alpha_\gamma^E$ (4)	$\alpha_\gamma^F$ (5)	Reference (6)
S5 0212+73	2.367	$0.32 \pm 0.19$	...	...	Sambruna et al. (2007)
PKS 0229+13	2.059	$0.39 \pm 0.09$	...	...	Marshall et al. (2005)
PKS 0413-21	0.808	$0.39 \pm 0.12$	...	...	Marshall et al. (2005)
PKS 0528+134	2.060	$0.12 \pm 0.26$	$1.46 \pm 0.04$	$1.54 \pm 0.09$	Donato et al. (2005)
PKS 0537-286	3.104	$0.27 \pm 0.02$	$1.47 \pm 0.60$	...	Reeves et al. (2001)
PKS 0745+241	0.409	$0.35 \pm 0.12$	...	...	Marshall et al. (2005)
SWIFT J0746.3+2548	2.979	$0.17 \pm 0.01$	...	...	Watanabe et al. (2009)
PKS 0805-07	1.837	$0.20 \pm 0.20$	$1.34 \pm 0.29(?)$	...	Giommi et al. (2007)
S5 0836+710	2.172	$0.34 \pm 0.04$	$1.62 \pm 0.16$	...	Donato et al. (2005)
RGB J0909+039	3.200	$0.26 \pm 0.12$	...	...	Giommi et al. (2002)
PKS 1127-145	1.184	$0.20 \pm 0.03$	$1.70 \pm 0.31$	$1.69 \pm 0.18$	Siemiginowska et al. (2008)
PKS 1424-41	1.522	$0.20 \pm 0.30$	$1.13 \pm 0.21$	...	Giommi et al. (2007)
GB 1428+4217	4.715	$0.29 \pm 0.05$	...	...	Fabian et al. (1998)
PKS 1510-089	0.360	$0.23 \pm 0.01$	$1.47 \pm 0.21$	$1.48 \pm 0.05$	Kataoka et al. (2008)
PKS 1830-211	2.507	$0.09 \pm 0.05$	$1.59 \pm 0.13$	...	De Rosa et al. (2005)
PKS 2149-306	2.345	$0.38 \pm 0.08$	...	...	Donato et al. (2005)
PKS 2223+210	1.959	$0.31 \pm 0.26$	...	...	Donato et al. (2005)
3C 454.3	0.859	$0.34 \pm 0.06$	$1.21 \pm 0.06$	$1.41 \pm 0.02$	Donato et al. (2005)

**Notes.** (1) Name of a source; (2) redshift of a source,  $z$ ; (3) X-ray spectral index,  $\alpha_x$ ; (4) EGRET  $\gamma$ -ray spectral index,  $\alpha_\gamma^E$  (Hartman et al. 1999); (5) *FERMI*  $\gamma$ -ray spectral index,  $\alpha_\gamma^F$  (Abdo et al. 2009b); and (6) references.

the cooling break in the electron distribution formed by such cascades, corresponding to the cooling break frequency in the synchrotron continuum  $\nu_{\text{syn},c}$  as measured in the observer frame, must correspond to the electron Lorentz factor

$$\gamma_c \simeq 6 \times 10^5 B'_G{}^{-1/2} \left( \frac{h\nu_{\text{syn},c}}{100 \text{ keV}} \right)^{1/2} \left( \frac{\Gamma}{20} \right)^{-1/2}, \quad (14)$$

where the comoving magnetic intensity is expressed in units of Gauss,  $B'_G \equiv B'/G$ . Meanwhile, equating the timescale of the synchrotron (electron) energy losses  $t'_{\text{cool}} \simeq \gamma/|\dot{\gamma}_{\text{syn}}|$  with the dynamical timescale of the emission region  $t'_{\text{dyn}} \simeq (R/c) \simeq r/(c\Gamma)$ , one may find

$$\gamma_c \simeq \frac{m_e c^2 \Gamma}{\sigma_T r u'_B}. \quad (15)$$

Hence, hard X-ray spectra observed in luminous blazars, if powered by hadronic interactions, require a jet magnetic field as low as

$$B'_G \simeq 5 \times 10^{-3} \left( \frac{\Gamma}{20} \right) \left( \frac{r}{\text{pc}} \right)^{-2/3} \left( \frac{h\nu_{\text{syn},c}}{100 \text{ keV}} \right)^{-1/3}. \quad (16)$$

However, in such weak magnetic fields, the SSC spectral component produced by copious, directly accelerated electrons can lead to the overproduction of the X-ray flux. In order to avoid this situation, the blazar emission zone must be located at sufficiently large distances to satisfy  $A = u'_{\text{syn}}/u'_B < q$ , where the comoving energy density of the the jet photons is

$$u'_{\text{syn}} \simeq \frac{L_{\text{syn}}}{4\pi r^2 c \Gamma^2} \simeq 7 \times 10^{-5} \left( \frac{L_{\text{syn}}}{10^{47} \text{ erg s}^{-1}} \right) \left( \frac{r}{\text{pc}} \right)^{-2} \times \left( \frac{\Gamma}{20} \right)^{-2} \text{ erg cm}^{-3}. \quad (17)$$

This condition, together with Equation (16), implies in turn

$$r > 20 \left( \frac{L_{\text{syn}}}{10^{47} \text{ erg s}^{-1}} \right)^{3/2} \left( \frac{h\nu_{\text{syn},c}}{100 \text{ keV}} \right) \left( \frac{\Gamma}{20} \right)^{-6} \times \left( \frac{q}{10} \right)^{-3/2} \text{ pc}. \quad (18)$$

At such distances, however, pair cascades are likely to be produced very inefficiently. In order to verify this, we calculate below the efficiency of the photo-meson process which dominates the powering of the cascades. The opacity for the photo-meson process involving protons with the random Lorentz factor  $\gamma_p$  is

$$\tau_{p\gamma}(\gamma_p) = \frac{t'^{-1}_{p\gamma}}{t'^{-1}_{\text{dyn}}} \simeq \langle \sigma_{p\gamma} K_{p\gamma} \rangle \frac{r n'_{\text{ph}}(\gamma_p)}{\Gamma}, \quad (19)$$

where  $\langle \sigma_{p\gamma} K_{p\gamma} \rangle \simeq 0.7 \times 10^{-28} \text{ cm}^2$  is the product of the photo-meson cross section and inelasticity parameter averaged over the resonant energy range (Begelman et al. 1990),  $n'_{\text{ph}}(\gamma_p) = \int_{\nu'_{\text{th}}(\gamma_p)} n'_{\text{ph},\nu'} d\nu'$  is the number density of photons with energies above the photo-meson threshold  $h\nu'_{\text{th}}(\gamma_p) \simeq m_\pi c^2/\gamma_p$ , and  $m_\pi c^2 \simeq 140 \text{ MeV}$  is the rest-mass energy of a pion. For  $\tau_{p\gamma}(\gamma_p) < 1$  (which can be verified a posteriori), the total efficiency of the process is

$$\eta_{p\gamma} = \frac{\int_1^{\gamma_{p,\text{max}}} \tau_{p\gamma} n'_{\gamma_p} \gamma_p d\gamma_p}{\int_1^{\gamma_{p,\text{max}}} n'_{\gamma_p} \gamma_p d\gamma_p}, \quad (20)$$

where  $n'_{\gamma_p}$  is the energy distribution of relativistic protons. The maximal available proton Lorentz factor, in turn,  $\gamma_{p,\text{max}}$ , may be evaluated very roughly through the condition  $t'_{\text{acc}}(\gamma_p) = t'_{\text{dyn}}$  (since the dynamical timescale is expected to be much shorter than any proton cooling timescale), where

$$t'_{\text{acc}}(\gamma_p) \simeq \frac{f R_L}{c} \simeq 10^{-4} \gamma_p f B'_G{}^{-1} \text{ s} \quad (21)$$

is the proton acceleration timescale,  $R_L \simeq \gamma_p m_p c^2 / (eB')$  is the proton Larmor radius, and the factor  $f$  accounts for the specific particle acceleration model assumed, being generally expected to be  $f \geq 10$  (see Aharonian et al. 2002). This, together with Equation (16), gives

$$\begin{aligned} \gamma_{p,\max} &\simeq 5 \times 10^9 B'_G \left(\frac{f}{10}\right)^{-1} \left(\frac{r}{\text{pc}}\right) \left(\frac{\Gamma}{20}\right)^{-1} \\ &\simeq 8 \times 10^7 \left(\frac{f}{10}\right)^{-1} \left(\frac{r}{20 \text{ pc}}\right)^{1/3} \left(\frac{h\nu_{\text{syn},c}}{100 \text{ keV}}\right)^{-1/3}, \end{aligned} \quad (22)$$

and the corresponding photon threshold energy is  $h\nu'_{\text{th}}(\gamma_{p,\max}) \sim (\gamma_{p,\max}/10^8)^{-1} \text{ eV}$ .

The target soft photons for the photo-meson production are provided by the synchrotron radiation of directly accelerated jet electrons, as well as by the external photon fields, dominated at parsec distances by hot/warm dust located in the surrounding molecular tori. The number density of synchrotron photons with energies larger than  $h\nu_{\text{th}}(\gamma_{p,\max})$  is

$$\begin{aligned} n'_{\text{syn}}(\gamma_{p,\max}) &\simeq \frac{L_{\text{syn}} \zeta(\gamma_{p,\max})}{4\pi r^2 c \Gamma^2 h\nu'_{\text{th}}(\gamma_{p,\max})} \simeq 5 \times 10^4 \zeta(\gamma_{p,\max}) \\ &\times \left(\frac{f}{10}\right)^{-1} \left(\frac{L_{\text{syn}}}{10^{47} \text{ erg s}^{-1}}\right) \left(\frac{r}{20 \text{ pc}}\right)^{-5/3} \\ &\times \left(\frac{\Gamma}{20}\right)^{-2} \left(\frac{h\nu_{\text{syn},c}}{100 \text{ keV}}\right)^{1/3} \text{ cm}^{-3}, \end{aligned} \quad (23)$$

where  $\zeta(\gamma_{p,\max}) \simeq L_{\text{syn}}(\nu > \Gamma \nu'_{\text{th}}(\gamma_{p,\max})) / L_{\text{syn}}$  which for the typical synchrotron spectra of luminous blazars and  $\gamma_{p,\max} \lesssim 10^8$  is expected to be  $\ll 1$ .

As for the external target photon field, we note that the dust located at  $r \sim 20 \text{ pc}$  and heated by the accretion disk with luminosity  $L_{\text{disk}} \sim 10^{46} \text{ erg s}^{-1}$  has a temperature  $T \sim 400 \text{ K}$  (see Equation (39)). Its electromagnetic spectrum peaks at  $h\nu_{\text{ext}} \simeq 0.1 \text{ eV}$ , and its comoving number density is

$$\begin{aligned} n'_{\text{ext}} &\simeq \Gamma n_{\text{ext}} \simeq 9 \times 10^7 \left(\frac{\xi_{\text{ext}}}{0.1}\right) \left(\frac{L_{\text{disk}}}{10^{46} \text{ erg s}^{-1}}\right) \left(\frac{\Gamma}{20}\right) \\ &\times \left(\frac{r}{20 \text{ pc}}\right)^{-2} \left(\frac{h\nu_{\text{ext}}}{0.1 \text{ eV}}\right)^{-1} \text{ cm}^{-3} \end{aligned} \quad (24)$$

(see Equation (40)). Hence, the target radiation field for the photo-meson process is dominated by the external radiation, and thus the opacity for protons with energies  $\gamma_p > \gamma_{p,\text{th}} \simeq m_\pi c^2 / (\Gamma h\nu_{\text{ext}})$  can be written as

$$\begin{aligned} \tau_{p\gamma}^{(\text{ext})} &\simeq 2 \times 10^{-2} \left(\frac{\xi_{\text{ext}}}{0.1}\right) \left(\frac{L_{\text{disk}}}{10^{46} \text{ erg s}^{-1}}\right) \left(\frac{r}{20 \text{ pc}}\right)^{-1} \\ &\times \left(\frac{h\nu_{\text{ext}}}{0.1 \text{ eV}}\right)^{-1}. \end{aligned} \quad (25)$$

For the most optimistic acceleration scenario with  $f = 10$ , and for the proton energy distribution of the form  $n'_{\gamma_p} \propto \gamma_p^{-2}$ , this gives the total efficiency

$$\eta_{p\gamma}^{(\text{ext})} \sim \tau_{p\gamma}^{(\text{ext})} \frac{\ln(\gamma_{p,\max}/\gamma_{p,\text{th}})}{\ln \gamma_{p,\max}} \sim 2 \times 10^{-4}. \quad (26)$$

With such a low efficiency of the photo-meson production process, the jet power required to explain the observed  $\gamma$ -ray luminosities of the order of  $10^{48} \text{ erg s}^{-1}$  is

$$\begin{aligned} L_j &\simeq \frac{L_\gamma}{\Gamma^2 \eta_{\text{diss}} \eta_p \eta_{p\gamma}} \simeq 5 \times 10^{50} \left(\frac{L_\gamma}{10^{48} \text{ erg s}^{-1}}\right) \left(\frac{\eta_{p\gamma}}{10^{-4}}\right)^{-1} \\ &\times \left(\frac{\eta_{\text{diss}}}{0.1}\right)^{-1} \left(\frac{\eta_p}{0.5}\right)^{-1} \text{ erg s}^{-1}, \end{aligned} \quad (27)$$

where  $\eta_{\text{diss}}$  is the fraction of the jet energy flux dissipated in the blazar emission zone, and  $\eta_p$  is the fraction of the dissipated energy channeled into relativistic protons. The required jet kinetic luminosity is therefore *orders of magnitude* larger than the Eddington luminosity of a black hole with a mass of  $10^9 M_\odot$ . Such serious energetic difficulties could be overcome only by postulating ad hoc some substructure of the blazar emission zone, involving spatial separation, and very different physical conditions characterizing regions where hadronic and leptonic processes operate. However, several arbitrary assumptions involved in such a scenario as well as an increased number of free parameters would make this much less attractive.

### 3.1.2. Proton-Synchrotron Emission

Alternatively, in order to explain hard X-ray spectra of luminous blazars still in the framework of hadronic models, one may postulate that the entire observed high-energy (X-ray-to- $\gamma$ -ray) flux is dominated by the direct synchrotron radiation of ultrarelativistic protons. Noting the relation between the characteristic proton- and electron-related synchrotron frequencies  $\nu_{p,\text{syn}}(\gamma_p = \gamma_e) = (m_e/m_p) \nu_{e,\text{syn}}$ , and the relation between the corresponding cooling rates  $|\dot{\gamma}_p|_{\text{syn}}(\gamma_p = \gamma_e) = (m_e/m_p)^3 |\dot{\gamma}_e|_{\text{syn}}$  (see, e.g., Aharonian 2000), one can find the appropriate radiative efficiency around the  $\gamma$ -ray luminosity peak:

$$\begin{aligned} \tau_{p,\text{syn}}(\gamma_{p,\text{peak}}) &\equiv \frac{t'^{-1}_{p,\text{syn}}}{t'^{-1}_{\text{dyn}}} \simeq 2 \times 10^{-4} B'_G{}^{3/2} \left(\frac{r}{\text{pc}}\right) \left(\frac{\Gamma}{20}\right)^{-3/2} \\ &\times \left(\frac{h\nu_{\text{peak}}}{10 \text{ MeV}}\right)^{1/2}, \end{aligned} \quad (28)$$

with

$$\gamma_{p,\text{peak}} \simeq 3 \times 10^8 B'_G{}^{-1/2} \left(\frac{h\nu_{\text{peak}}}{10 \text{ MeV}}\right)^{1/2}. \quad (29)$$

The resulting efficiency of the synchrotron proton emission is, again, very low, and can be increased only by assuming very large magnetic field intensity within the emission zone. However, since the magnetic energy flux is limited by the total jet kinetic power,  $L_B \simeq cu'_B \pi r^2 < L_j$ , magnetic fields  $B'_G \gg 1$  are expected only at  $r \ll 1 \text{ pc}$ . In this context, one has to keep in mind that at small distances from the black hole, AGN jets are still in the acceleration phase, and thus the radiation produced there is not boosted sufficiently strongly to account for the observed large luminosities. The distance scale of the jet acceleration, which corresponds roughly with the distance of the conversion of the Poynting flux dominated jet to that dominated by matter, is expected to be  $r_0 \geq 10^3 R_g \simeq 0.03 (M_{\text{BH}}/10^9 M_\odot) \text{ pc}$  (Komissarov et al. 2007), where  $R_g$  is the radius of the central black hole. Considering those additional constraints,

we obtain

$$\tau_{p,\text{syn}}(\gamma_{p,\text{peak}}) < 2 \times 10^{-3} \left( \frac{r_0}{0.03 \text{ pc}} \right)^{-1/2} \left( \frac{\Gamma}{20} \right)^{-3/2} \times \left( \frac{h\nu_{\text{peak}}}{10 \text{ MeV}} \right)^{1/2} \left( \frac{L_j}{10^{47} \text{ erg s}^{-1}} \right)^{3/4}, \quad (30)$$

where  $L_j \sim 10^{47} \text{ erg s}^{-1}$  corresponds to the Eddington luminosity of the  $10^9 M_\odot$  black hole. With such an efficiency, the proton synchrotron peak luminosity is

$$L_{p,\text{syn}}(10 \text{ MeV}) < 4 \times 10^{45} \left( \frac{\eta_{\text{diss}}}{0.1} \right) \left( \frac{\eta_p}{0.5} \right) \left( \frac{\tau_{p,\text{syn}}}{2 \times 10^{-3}} \right) \times \left( \frac{\Gamma}{20} \right)^2 \left( \frac{L_j}{10^{47} \text{ erg s}^{-1}} \right) \text{ erg s}^{-1}, \quad (31)$$

i.e., orders of magnitude below the observed  $\gamma$ -ray luminosity of powerful blazars.

### 3.2. Hard X-ray Spectra in the SSC Model

In the SSC model for large- $q$  blazars, the electron cooling rate is dominated by Comptonization of cospatially produced synchrotron radiation, and therefore reads as

$$|\dot{\gamma}| \simeq |\dot{\gamma}|_{\text{SSC}} \simeq \frac{c\sigma_T \gamma^2 u'_{\text{syn}}}{m_e c^2}, \quad (32)$$

where

$$u'_{\text{syn}} \simeq \frac{L_{\text{syn}}}{4\pi R^2 c \Gamma^4}. \quad (33)$$

Balancing next the corresponding comoving timescale of radiative losses  $t'_{\text{cool}} \simeq \gamma/|\dot{\gamma}|_{\text{SSC}}$  with the dynamical timescale of the emission region  $t'_{\text{dyn}}$ , one may find the critical electron energy corresponding to the transition between fast- and slow-cooling regimes:

$$\gamma_c \simeq 10^5 \left( \frac{\Gamma}{20} \right)^3 \left( \frac{r}{\text{pc}} \right) \left( \frac{L_{\text{syn}}}{10^{47} \text{ erg s}^{-1}} \right)^{-1}. \quad (34)$$

Electrons with  $\gamma < \gamma_c$  cool inefficiently, Compton upscattering the far-infrared synchrotron radiation up to MeV photon energies. Therefore, the observed hard X-ray spectra can be reproduced by the SSC model in a framework of the standard approach involving injection of some given (single or broken) power-law electron energy distribution to the emission region and its subsequent radiative cooling, provided the low-energy segment of the injected electron energy distribution is not softer than  $\propto \gamma^{-2}$ .

### 3.3. Hard X-ray Spectra in the EC Models

In the EC models for blazars with large values of the  $q$  parameter, radiative cooling of electrons is dominated by Comptonization of the external radiation fields. As before, by equating the appropriate cooling timescale

$$t'_{\text{cool}} \simeq \frac{m_e c^2}{\gamma c \sigma_T u'_{\text{ext}}} \quad (35)$$

with the dynamical timescale of the emission region  $t'_{\text{dyn}}$ , one finds the critical electron Lorentz factor

$$\gamma_c \simeq \frac{m_e c^2 \Gamma}{\sigma_T u'_{\text{ext}} r}, \quad (36)$$

where we assumed that the energy density of the external photon field may be approximated as being constant up to some characteristic distance  $r_{\text{ext}}$ , and that the blazar emission zone is located at  $r_0 < r \leq r_{\text{ext}}$ , where  $r_0$  is the distance scale of the jet acceleration (see Section 3.1.2).

In the case of the dominant EC(BLR) emission, i.e., when the electron cooling is dominated by Comptonization of the photon field due to the broad emission lines, we have  $r_0 < r \leq r_{\text{ext}} = r_{\text{BLR}}$ , where

$$r_{\text{BLR}} \simeq 0.1 \left( \frac{L_{\text{disk}}}{10^{46} \text{ erg s}^{-1}} \right)^{1/2} \text{ pc} \quad (37)$$

(Ghisellini & Tavecchio 2008 and references therein) and

$$u'_{\text{ext}} \simeq u_{\text{BLR}} \Gamma^2 \simeq \frac{\xi_{\text{BLR}} L_{\text{disk}} \Gamma^2}{4\pi r_{\text{BLR}}^2 c} \simeq 12 \left( \frac{\xi_{\text{BLR}}}{0.1} \right) \left( \frac{\Gamma}{20} \right)^2 \text{ erg cm}^{-3}. \quad (38)$$

If, instead,  $r_{\text{BLR}} < r < r_{\text{HDR}}$ , where

$$r_{\text{HDR}} \simeq 4 \left( \frac{L_{\text{disk}}}{10^{46} \text{ erg s}^{-1}} \right)^{1/2} \left( \frac{T}{10^3 \text{ K}} \right)^{-2.6} \text{ pc}, \quad (39)$$

the electron cooling is dominated by IC upscattering of the near-IR photons emitted by the hot dust with the temperature  $T$ , located in the molecular torus and irradiated by the accretion disk (Nenkova et al. 2008, and references therein). In such a case

$$u'_{\text{ext}} \simeq u_{\text{HDR}} \Gamma^2 \simeq \frac{\xi_{\text{HDR}} L_{\text{disk}} \Gamma^2}{4\pi r_{\text{HDR}}^2 c} \simeq 8 \times 10^{-3} \left( \frac{T}{10^3 \text{ K}} \right)^{5.2} \times \left( \frac{\xi_{\text{HDR}}}{0.1} \right) \left( \frac{\Gamma}{20} \right)^2 \text{ erg cm}^{-3}, \quad (40)$$

and the EC(HDR) emission dominates the high-energy radiative output of the source.

With all the values quoted above, the critical electron Lorentz factor reads as

$$\gamma_c \simeq \left( \frac{\Gamma}{20} \right)^{-1} \left( \frac{L_{\text{disk}}}{10^{46} \text{ erg s}^{-1}} \right)^{-1/2} \times \begin{cases} 7 (r/r_{\text{BLR}})^{-1} (\xi_{\text{BLR}}/0.1)^{-1} \\ 250 (r/r_{\text{HDR}})^{-1} (\xi_{\text{HDR}}/0.1)^{-1} (T/10^3 \text{ K})^{-2.6}, \end{cases} \quad (41)$$

and the corresponding break frequency in the high-energy spectral component,  $\nu_{\text{EC},c} \simeq \gamma_c^2 \Gamma^2 \nu_{\text{ext}}$ , may be evaluated as

$$\left( \frac{h\nu_{\text{EC},c}}{\text{MeV}} \right) \simeq \left( \frac{L_{\text{disk}}}{10^{46} \text{ erg s}^{-1}} \right)^{-1} \times \begin{cases} 0.2 (r/r_{\text{BLR}})^{-2} (\xi_{\text{BLR}}/0.1)^{-2} \\ 8 (r/r_{\text{HDR}})^{-2} (\xi_{\text{HDR}}/0.1)^{-2} (T/10^3 \text{ K})^{-5.2}, \end{cases} \quad (42)$$

where  $h\nu_{\text{ext}}$  has been substituted with  $h\nu_{\text{BLR}} \simeq 10 \text{ eV}$  and  $h\nu_{\text{HDR}} \simeq 0.3 \text{ eV}$ , respectively. Hence, the production of high-energy emission in the EC(HDR) model proceeds in the slow-cooling regime up to the MeV photon energy range, in agreement with the position of luminosity peaks observed in luminous

blazars. In the EC(BLR) model, the  $\gamma$ -ray spectra are expected to soften below the MeV range, but still at sufficiently high photon energies to assure consistency with observations. Hence, in similarity to the case of the SSC model, the observed very hard X-ray spectra of powerful blazar sources are in agreement with the EC scenario for the high-energy jet emission.

High-energy radiation produced in the innermost portions of AGN jets may also be contributed by Comptonization of the direct emission of the accretion disk illuminating the blazar emission zone from the sides and from behind. This contribution should in particular dominate the high-energy radiative output of the jet at distances:

$$r < r_{\text{disk/BLR}} \simeq 0.6 \left( \frac{r_{\text{BLR}}^2 R_g}{\xi_{\text{BLR}}} \right)^{1/3} \simeq 0.01 \left( \frac{\xi_{\text{BLR}}}{0.1} \right)^{-1/3} \times \left( \frac{L_{\text{disk}}}{10^{46} \text{ erg s}^{-1}} \right)^{1/3} \left( \frac{M_{\text{BH}}}{10^9 M_\odot} \right)^{1/3} \text{ pc} \quad (43)$$

(Dermer & Schlickeiser 2002). Energy dissipation events taking place on such small scales may be responsible for the production of intraday flares observed sporadically in some blazar sources (see Section 7.2).

#### 4. SYNCHROTRON AND INVERSE-COMPTON PEAK FREQUENCIES

In the case of luminous blazars, the observed synchrotron peak frequencies seem to cluster within a relatively narrow frequency range  $10^{12}$ – $10^{14}$  Hz (Ghisellini & Tavecchio 2008 and references therein). Meanwhile, the peak of the high-energy spectral components of the objects discussed here has to be located between 0.1 MeV and 0.1 GeV photon energies, as indicated by the observed values of the X-ray and  $\gamma$ -ray spectral indices (e.g., Fossati et al. 1998; Ghisellini & Tavecchio 2008). Again, the relative location of the low- and high-energy spectral peaks does not provide any constraints on the hadronic models, because the poorly known particle acceleration efficiency (the  $f$  parameter introduced in Equation (21)) is claimed to be substantially different for electrons and protons (e.g., Reimer et al. 2004), and therefore the ratio of peak frequencies is in fact a free parameter. However, in the leptonic scenarios for the high-energy blazar emission, the relative location of spectral peaks offers interesting constraints on the model parameters, as discussed below.

##### 4.1. Peak Frequencies in the SSC Model

Peak frequencies of the synchrotron and SSC components in the spectra of blazar sources are determined by the critical (break) energies of electrons emitting bulk of the emission,

$$\gamma_{\text{br}} \simeq \sqrt{\frac{v_{\text{SSC,br}}}{v_{\text{syn,br}}}}. \quad (44)$$

When combined with the standard formulae for the corresponding break frequency of the synchrotron photons

$$v_{\text{syn,br}} \simeq 4 \times 10^6 B'_G \gamma_{\text{br}}^2 \Gamma \text{ Hz}, \quad (45)$$

we obtain

$$h\nu_{\text{SSC,br}} = 10^{18} B'_G{}^{-1} \left( \frac{v_{\text{syn,br}}}{10^{13} \text{ Hz}} \right)^2 \left( \frac{\Gamma}{20} \right)^{-1} \text{ Hz}. \quad (46)$$

In the SSC model, magnetic field intensity  $B'$  given by the relation  $u'_{\text{syn}}/u'_B \simeq q$  is

$$B'_G \simeq 10^{-2} \left( \frac{L_{\text{syn}}}{10^{47} \text{ erg s}^{-1}} \right)^{1/2} \left( \frac{\Gamma}{20} \right)^{-1} \left( \frac{r}{\text{pc}} \right)^{-1} \left( \frac{q}{10} \right)^{-1/2}, \quad (47)$$

and hence

$$h\nu_{\text{SSC,br}} \simeq 0.4 \left( \frac{v_{\text{syn,br}}}{10^{13} \text{ Hz}} \right)^2 \left( \frac{\Gamma}{20} \right) \left( \frac{r}{\text{pc}} \right) \left( \frac{q}{10} \right)^{1/2} \times \left( \frac{L_{\text{syn}}}{10^{47} \text{ erg s}^{-1}} \right)^{-1/2} \text{ MeV}. \quad (48)$$

This would then be consistent with the observational constraints for the location of the emitting zone  $r >$  a few pc.

However, the SSC mechanism can dominate the production of the  $\gamma$ -ray emission only if the energy density of synchrotron radiation is larger than the energy density of the external radiation field, both as measured in the source comoving frame, i.e., if  $u'_{\text{syn}} > u'_{\text{ext}} \simeq u_{\text{ext}} \Gamma^2$ . This condition can be satisfied on parsec scales, provided the contribution from the BLR at these distances is already negligible (as expected even in luminous blazars) and the dust temperature is much below the sublimation temperature. The second requirement can be verified observationally by investigating the presence of a hot dust in mid- and near-IR data for non-blazar radio-loud quasars, i.e., for jet sources observed at  $\theta_{\text{obs}} \gg 1/\Gamma$ . According to Cleary et al. (2007), who analyzed *Spitzer* observations of 3C quasars, the dust temperatures are in the range,  $T \sim 100$ – $300$  K. Such temperatures are derived assuming that the observed mid-IR excess in the spectra of analyzed objects is produced by a high-energy tail of the synchrotron radiation of a large-scale jet. If this is indeed the case, then there is a distance range between  $r_{\text{BLR}}$  and  $r_{\text{HDR}}$  where the SSC process can dominate the production of  $\gamma$ -rays over the EC(HDR) mechanism. On the other hand, we note that the near-IR quasar continua join the harder optical ones almost always around the same frequency, namely  $\sim 1 \mu\text{m}$ , in both radio-quiet and radio-loud sources (Barvainis 1987; Glikman et al. 2006; Netzer et al. 2007; Labita et al. 2008). Therefore, the assumption regarding the synchrotron origin of near-IR radiation seems not to be justified, requiring in addition very precise tuning of the jet parameters. At the same time, a natural explanation for the observed spectral dip around  $1 \mu\text{m}$  frequencies in quasar spectra is provided by the clumpy torus model, in a framework of which the near-IR emission is produced by a hot dust with the temperature close to the sublimation value,  $T \sim 1500$  K (Nenkova et al. 2008).

##### 4.2. Peak Frequencies in the EC Models

In the EC models, the high-energy (IC) spectral component is expected to peak at the observed frequencies

$$\nu_{\text{EC,br}} \simeq \gamma_{\text{br}}^2 \Gamma^2 \nu_{\text{ext}}, \quad (49)$$

and the ratio of the peak frequencies reads

$$\frac{\nu_{\text{EC,br}}}{\nu_{\text{syn,br}}} \simeq 10^9 \left( \frac{\Gamma}{20} \right) \left( \frac{h\nu_{\text{ext}}}{\text{eV}} \right) B'_G{}^{-1}. \quad (50)$$

With the magnetic field given by the  $q = \Gamma^2 u_{\text{ext}}/u'_B$  condition,

$$B'_G = \Gamma \sqrt{\frac{8\pi}{q}} \left( \frac{u_{\text{ext}}}{\text{erg cm}^{-3}} \right)^{1/2} \simeq \left( \frac{\Gamma}{20} \right) \left( \frac{q}{10} \right)^{-1/2} \times \begin{cases} 5 (\xi_{\text{BLR}}/0.1)^{1/2} \\ 0.1 (\xi_{\text{HDR}}/0.1)^{1/2} (T/10^3 \text{ K})^{2.6}, \end{cases} \quad (51)$$

this ratio is then surprisingly similar for both cases considered here, EC(BLR) and EC(HDR):

$$\frac{v_{\text{EC, br}}}{v_{\text{syn, br}}} \simeq 3 \times 10^9 \left( \frac{q}{10} \right)^{1/2} \times \begin{cases} (\xi_{\text{BLR}}/0.1)^{-1/2} \\ (\xi_{\text{HDR}}/0.1)^{-1/2} (T/10^3 \text{ K})^{-2.6}, \end{cases} \quad (52)$$

leading to the expected spectral location of the EC luminosity peak,

$$h\nu_{\text{EC, br}} \simeq 0.1 \left( \frac{q}{10} \right)^{1/2} \left( \frac{\xi_{\text{ext}}}{0.1} \right)^{-1/2} \left( \frac{v_{\text{syn, br}}}{10^{13} \text{ Hz}} \right) \text{ GeV}, \quad (53)$$

with the assumed  $T \sim 10^3 \text{ K}$ . The  $h\nu_{\text{EC, br}}$  evaluated above seems to be somewhat higher than the peak photon energies of the high-energy continua claimed for luminous blazars (Ghisellini & Tavecchio 2008), as long as  $v_{\text{syn, br}}$  is not smaller than  $10^{13} \text{ Hz}$ . However, we note that the high-energy peak frequencies are not observed directly, but only reconstructed from the power-law slopes of the lower-energy (X-ray) and higher-energy (GeV) segments of the IC continua, assuming a single-broken power-law spectral shape of the emission. Meanwhile, if the injected electron spectrum is flatter than  $\gamma^{-2}$  below electron energies  $\gamma_{\text{br}}$  corresponding to the peak frequencies  $v_{\text{syn, br}}$  and  $v_{\text{EC, br}}$  (as seems to be indicated by the observed hard X-ray spectra with  $\alpha_x < 0.5$ ), and steeper than that above  $\gamma_{\text{br}}$  (see in this context Ghisellini & Tavecchio 2008, but also Section 9 of this paper), the “reconstructed” peak frequency can easily be lower than the “true” break frequency  $v_{\text{EC, br}}$  by a factor of  $(v_{\text{EC, c}}/v_{\text{EC, br}})^{(0.5-\alpha_x)/(\alpha_\gamma-\alpha_x)}$ , i.e., by possibly as much as  $\sim 10$  for the typical values of the X-ray and GeV spectral indices of luminous blazars (see Table 1).

## 5. LACK OF BULK-COMPTON SPECTRAL FEATURES

In astrophysical jets, *all* ultrarelativistic particles cool due to radiative energy losses and also due to adiabatic expansion of the emitting regions. Hence, the observed high-energy non-thermal radiation requires in situ particle acceleration, and one may expect to observe at any given instant radiation from both “cold” and “hot” population of particles. Typically, jet electrons constituting a cold population are considered to be nonrelativistic in the jet rest frame in the innermost parts of the outflow (say, hundreds of Schwarzschild radii from the active center), because of the extremely rapid (catastrophic) particle cooling at the jet base. Such electrons, if indeed present in a steady flow, are predicted to produce distinct bulk-Compton features in blazar spectra, most pronounced around  $h\nu_{\text{bc}} \sim \Gamma^2 h\nu_{\text{ext}}$  photon energies, i.e., around  $\sim 1\text{--}4 \text{ keV}$  for  $\Gamma \sim 10\text{--}20$  and  $h\nu_{\text{ext}} \sim 10 \text{ eV}$  (Begelman & Sikora 1987; Sikora et al. 1997; Sikora & Madejski 2000). In addition, in the internal shock model (Spada et al. 2001), the presence of cold jet electrons should manifest itself as soft and hard X-ray precursors of non-thermal blazar flares (Moderski et al. 2004). Both those “steady” and “dynamic” bulk-Compton features are expected to be particularly strong if produced close to the black

hole, in the dense radiation field of an accretion disk. So far, no clear detection of such features has been reported, with the possible exception of weak soft X-ray excesses claimed in the spectra of some blazars (see, e.g., Worsley et al. 2004; Kataoka et al. 2008; De Rosa et al. 2008). Such an apparent weakness of bulk-Compton features may result from the fact that in the very central regions of AGN jet the (magnetohydrodynamical, MDH) acceleration of the outflow is not yet fully complete (as noted previously in Sikora et al. 2005; Celotti et al. 2007). On the other hand, analogous spectral features produced further out at the point where the jet is already accelerated to terminal bulk velocities are predicted to be still detectable, in particular if the blazar emission zone is enclosed within the BLR.

However, it should be emphasized that the involved assumptions regarding cold electron population may not be valid at all scales. Namely, at some larger distances from the nucleus, the radiative and adiabatic cooling are expected to become inefficient when compared to the acceleration processes at very low electron energies. As a result, shock heating and/or interaction of particles with magnetic turbulence (driven inevitably by MHD instabilities of a magnetized outflow, and the related magnetic reconnection processes) may effectively accelerate all the cold electrons to energies  $\gamma \gg 1$ , replacing the nonrelativistic Maxwellian-like electron population with a very hard, quasi-power-law distribution that joins smoothly the higher-energy electron tail (see Section 9). In such a case, bulk-Compton features are expected to be absent. Yet another alternative explanation for the apparent lack of radiative signatures of cold electrons in blazar spectra is that the formation and acceleration of jets in luminous sources are still not completed within the BLR. If so, bulk-Compton features produced at  $r < r_{\text{BLR}}$  may be simply too weak to be distinguished from the broadband continuum generated via the EC(HDR) process. The latter possibility is supported by the fact that in several cases pure power-law X-ray continua extend down to energies  $0.1\text{--}0.3 \text{ keV}$ , with no evidence for any soft excess (e.g., in 3C 279; see Lawson & McHardy 1998; Collmar et al. 2007).

## 6. LACK OF KLEIN–NISHINA SPECTRAL FEATURES

Recent studies of the KN effects of relativistic sources immersed in a dense external radiation field and dominated by the IC emission show that for the maximum electron energies  $\gamma_{\text{max}} \gg \gamma_{\text{KN}} \equiv m_e c^2 / 4\Gamma h\nu_{\text{ext}}$  the IC continuum should break at much larger frequencies than  $\nu_{\text{KN}} = \gamma_{\text{KN}}^2 \Gamma^2 \nu_{\text{ext}}$ , and that the synchrotron component should harden around

$$\nu_{\text{syn, KN}} \simeq 4 \times 10^6 \gamma_{\text{KN}}^2 \Gamma B'_G \text{ Hz} \simeq 3 \times 10^{15} B'_G \times \left( \frac{\Gamma}{20} \right)^{-1} \left( \frac{h\nu_{\text{ext}}}{\text{eV}} \right)^{-2} \text{ Hz} \quad (54)$$

(Dermer & Atoyan 2002; Moderski et al. 2005). Both these effects result from hardening of the injected electron energy distribution due to the reduction of the IC cooling rate in the KN regime, i.e., for the electrons with  $\gamma > \gamma_{\text{KN}}$ . In a framework of the EC(BLR) model, the related spectral features are expected to be pronounced already for electrons with energies  $\gamma > 3 \times 10^3$ , and the hardening of the synchrotron continuum (being especially strong for monoenergetic external radiation fields) is predicted to be visible already in the optical band. However, as shown by Tavecchio & Ghisellini (2008), emission of BLR is not exactly monochromatic, and in particular is characterized by a significant low-frequency power-law tail.

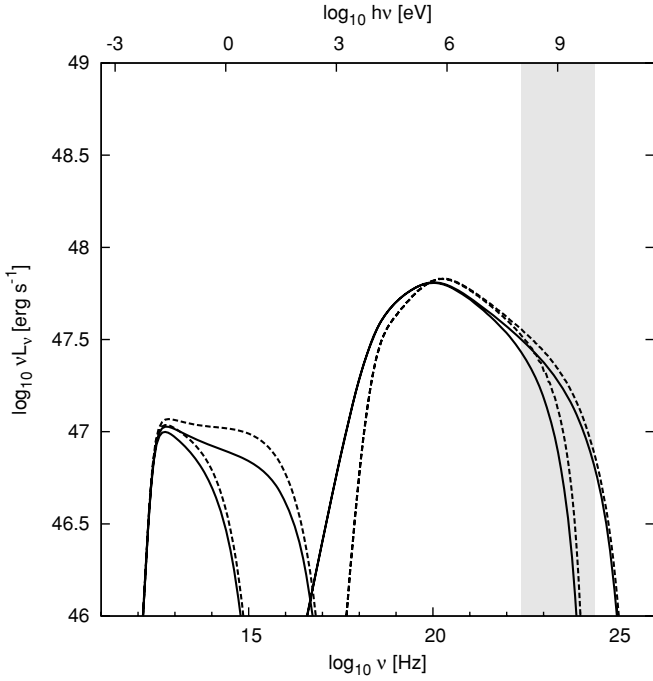


**Figure 1.** Broadband spectra of fiducial blazars showing the KN effects for the EC(BLR) model. Solid lines are calculated for a power-law-type external radiation with photon index  $\alpha = 0$ , while dashed lines show models with monochromatic external radiation (approximated by blackbody-type emission). Two families of models are shown, corresponding to the injection of the electron energy distribution  $N_\gamma \propto \gamma^{-2.4}$  with maximal electron energies  $\gamma_{\max} = 10^3$  and  $10^4$  (lower and upper curves, respectively). All models are calculated for  $q = 10$ . The shaded area indicates the energy range observable by the *Fermi*/LAT.

As a result, the expected KN hardening in the optical band may be relatively weak, though possibly still prominent in the UV band. The dependence of such KN effects on the maximum electron energy and the parameter  $q$  for the EC(BLR) model is illustrated in Figures 1 and 2, with an assumed electron energy distribution  $N_\gamma \propto \gamma^{-s}$  with  $s = 2.4$ . As shown in these figures, high- $q$  blazars with synchrotron and IC spectra extending respectively above 1 eV and 10 GeV photon energies should display in their broadband continua the KN spectral features discussed above, *unless* the production of  $\gamma$ -rays is dominated by Comptonization of IR radiation of hot dust, and *only if* the electron energy distribution extends to  $\gamma > 3 \times 10^3$  with the power-law slope not much steeper than  $s \simeq 2.5$ . This provides a possibility of determining the characteristic energies of the dominant seed photons via the analysis of the KN effects, manifested by different spectral shapes of the high-energy tails of the synchrotron and EC continua.

## 7. EC(HDR) VERSUS EC(BLR) MODELS

As shown in Section 4, the same luminosity ratio of the IC and synchrotron spectral components implies similar high-energy peak frequencies in both EC(BLR) and EC(HDR) models. And this is clearly coincidental since the location of the two spectral peaks happens to scale with a factor  $v_{\text{ext}}/\sqrt{u_{\text{ext}}}$  (see Section 3.3). Interestingly, the conspiracy between the two models is reflected also by several other—though not by all—important model output parameters, as discussed below.

### 7.1. Similarities

Let us consider a “fiducial” source located within a given distance range  $\Delta r \sim r$ , and immersed in a given external

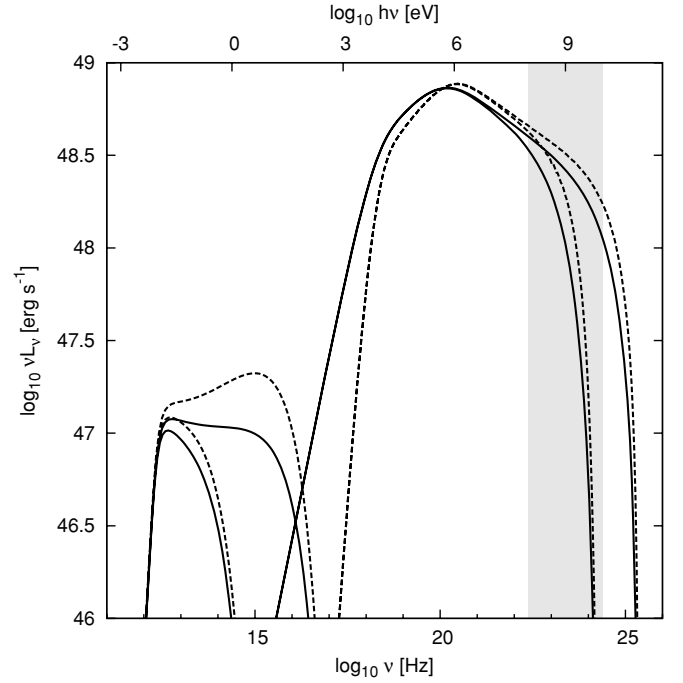


**Figure 2.** Same as Figure 1, but with  $q = 100$ .

radiation field. The observed X-ray and  $\gamma$ -ray spectral indices of such a source,  $\alpha_x$  and  $\alpha_\gamma$  respectively, allow one to reconstruct the energy distribution of radiating electrons, approximated here for simplicity by a single-broken power law. In particular, using the approximate formula

$$L_\nu d\nu \simeq N_\gamma d\gamma |\dot{\gamma}| m_e c^2 \Gamma^4, \quad (55)$$

we find that

$$N_\gamma = C_{N_1} \gamma^{-s_1} (1 + \gamma/\gamma_{\text{br}})^{s_1 - s_2}, \quad (56)$$

$$\gamma_{\text{br}} = \left( \frac{C_{N_2}}{C_{N_1}} \right)^{1/(s_1 - s_2)}, \quad (57)$$

$$C_{N_1} \simeq \frac{2v_{\text{ext}}^{1-\alpha_x}}{c\sigma_T u_{\text{ext}} \Gamma^{4+2\alpha_x}} C_x, \quad (58)$$

$$C_{N_2} \simeq \frac{2v_{\text{ext}}^{1-\alpha_\gamma}}{c\sigma_T u_{\text{ext}} \Gamma^{4+2\alpha_\gamma}} C_\gamma, \quad (59)$$

$$C_x = \frac{[v_x L_{v_x}]}{v_x^{1-\alpha_x}} = \frac{4\pi d_L^2 [v_{\text{obs}, x} F_{v_{\text{obs}, x}}]}{v_{\text{obs}, x}^{1-\alpha_x}}, \quad (60)$$

$$C_\gamma = \frac{[v_\gamma L_{v_\gamma}]}{v_\gamma^{1-\alpha_\gamma}} = \frac{4\pi d_L^2 [v_{\text{obs}, \gamma} F_{v_{\text{obs}, \gamma}}]}{v_{\text{obs}, \gamma}^{1-\alpha_\gamma}}, \quad (61)$$

$$s_1 = 2\alpha_x + 1, \quad \text{and} \quad s_2 = 2\alpha_\gamma + 1. \quad (62)$$

Here  $F_{v_{\text{obs}}}$  are the observed monochromatic energy fluxes at some particular observed frequency  $v_{\text{obs}}$ ,  $d_L$  is the luminosity distance of the source, and  $z$  is its redshift.

The number of electrons contributing to the radiation at a given instant of observation can be approximated by

$$N_e = \int_1 N_\gamma d\gamma \simeq \frac{C_{N_1}}{2\alpha_x}, \quad (63)$$

as long as  $\gamma_{\text{br}} \gg 1$  and  $\gamma_{\text{min}} = 1$ . Hence, the electron number flux is

$$\dot{N}_e \simeq \frac{N_e}{(R/\Gamma c)} \simeq \frac{\Gamma^2 N_e}{(r_{\text{ext}}/c)} \propto \frac{v_{\text{ext}}^{1-\alpha}}{u_{\text{ext}} r_{\text{ext}}}, \quad (64)$$

and the ratio of electron energy fluxes in the two considered models reads as

$$\begin{aligned} \frac{\dot{N}_{e,\text{HDR}}}{\dot{N}_{e,\text{BLR}}} &\simeq \left( \frac{v_{\text{HDR}}}{v_{\text{BLR}}} \right)^{1-\alpha_x} \left( \frac{u_{\text{HDR}}}{u_{\text{BLR}}} \right)^{-1} \left( \frac{r_{\text{HDR}}}{r_{\text{BLR}}} \right) \\ &\simeq 6 \left( \frac{T}{10^3 \text{ K}} \right)^{-2.6} \left( \frac{\xi_{\text{HDR}}}{\xi_{\text{BLR}}} \right)^{-1}, \end{aligned} \quad (65)$$

which, for the sublimation temperature  $T \simeq 1500 \text{ K}$  and  $\xi_{\text{HDR}} \sim 3 \xi_{\text{BLR}}$ , is of the order of unity.

Assuming further that the energy flux of a jet is dominated by nonrelativistic protons, the proton number flux is simply

$$\dot{N}_p \simeq \frac{L_j}{\Gamma m_p c^2}, \quad (66)$$

and therefore the pair content in the two models is

$$\frac{(n_e/n_p)_{\text{HDR}}}{(n_e/n_p)_{\text{BLR}}} = \frac{\dot{N}_{e,\text{HDR}}}{\dot{N}_{e,\text{BLR}}}, \quad (67)$$

i.e., almost exactly the same. In addition, a similar value for  $\dot{N}_e$  derived for the two models implies also similar electron energy fluxes:

$$L_e = \langle \gamma \rangle m_e c^2 \Gamma \dot{N}_e, \quad (68)$$

where  $\langle \gamma \rangle = \int N_\gamma \gamma d\gamma / \int N_\gamma d\gamma \simeq \ln \gamma_{\text{br}}$  is the average electron Lorentz factor (assuming  $\alpha_x \simeq 0.5$ ), and  $\gamma_{\text{br}} = \Gamma^{-1} \sqrt{v_{\text{EC, br}}/v_{\text{ext}}}$ . It follows directly from the above discussion (Sections 3 and 4) that  $\langle \gamma \rangle$ , and thus  $L_e$ , is the same for the EC(BLR) and EC(HDR) models. Finally, also magnetic energy fluxes  $L_B \simeq cu'_B \Gamma^2 \pi R^2 \sim cu'_B \pi r^2$  do not differ in both cases considered above, namely

$$\frac{L_{B,\text{HDR}}}{L_{B,\text{BLR}}} = \frac{u_{\text{HDR}} r_{\text{HDR}}^2}{u_{\text{BLR}} r_{\text{BLR}}^2} = 0.65 \left( \frac{T}{10^3 \text{ K}} \right)^{2.6} \frac{\xi_{\text{HDR}}}{\xi_{\text{BLR}}}. \quad (69)$$

### 7.2. Differences

Certainly, there are some aspects which differentiate the two models considered. These are (1) the critical synchrotron self-absorption frequencies, (2) the characteristic variability timescales, and (3) the low-energy breaks/cutoffs of the IC spectral component.

1. The synchrotron self-absorption makes the source optically thick below the frequency

$$\begin{aligned} \nu_a &\simeq 4 \times 10^{11} B_G'^{1/7} \left( \frac{[v_a L_{v_a}]}{10^{47} \text{ erg s}^{-1}} \right)^{2/7} \\ &\times \left( \frac{\Gamma}{20} \right)^{3/7} \left( \frac{r}{\text{pc}} \right)^{-4/7} \text{ Hz}, \end{aligned} \quad (70)$$

which may be re-written as

$$\begin{aligned} \left( \frac{\nu_a}{10^{12} \text{ Hz}} \right) &\simeq \left( \frac{[v_a L_{v_a}]}{10^{47} \text{ erg s}^{-1}} \right)^{2/7} \\ &\times \begin{cases} 2 (B'/5 \text{ G})^{1/7} (r/r_{\text{BLR}})^{-4/7} \\ 0.2 (B'/0.1 \text{ G})^{1/7} (r/r_{\text{HDR}})^{-4/7} \end{cases}. \end{aligned} \quad (71)$$

Meanwhile, millimeter and submillimeter observations indicate absorption break in blazar spectra around 1 mm (see, e.g., Gear et al. 1994). This favors the EC(HDR) model over the EC(BLR) version.

2. The shortest timescales of flares differ in the two EC models by a factor  $r_{\text{HDR}}/r_{\text{BLR}} \sim 30 (T/10^3 \text{ K})^{-2.6}$ . In particular, one has

$$\begin{aligned} \left( \frac{t_{\text{min}}}{\text{day}} \right) &\simeq \left( \frac{L_{\text{disk}}}{10^{46} \text{ erg s}^{-1}} \right) \left( \frac{\Gamma}{20} \right)^{-2} \\ &\times \begin{cases} 0.4 \\ 10 (T/10^3 \text{ K})^{-2.6} \end{cases}. \end{aligned} \quad (72)$$

Hence, the characteristic variability timescale predicted by the EC(HDR) model is more consistent with the one implied by the observed variability patterns in “optically violent variable” quasars, which is of the order of days/weeks (Pica et al. 1988). A nice example where such timescales are seen both in the  $\gamma$ -ray and IR/optical frequency ranges is provided by multiwavelength observations of blazar 3C 454.3 (see Figure 1 in Bonning et al. 2009).

We note in this context that in some cases rapid, day/intraday flares are imposed on the observed light curves of blazar sources. One example is the extremely rapid ( $\sim 2 \text{ hr}$ ) optical flare, as recorded also in 3C 454.3 (Raiteri et al. 2008), or intraday  $\gamma$ -ray flare recorded by *Fermi*/LAT in the radio quasar PKS 1454–354 (Abdo et al. 2009a). Such rapid flares may indicate that in addition to the main “energy dissipation site” located at parsec-scale distances from the active center, there are also episodic dissipation events taking place on sub-parsec distances, possibly related to MHD instabilities and/or internal shocks within the inner parts of a strongly magnetized outflow.

3. Because the spectra produced by relativistic electrons emerge at energies  $h\nu_{\text{low}} \simeq \Gamma^2 v_{\text{ext}}$ , in the case of the EC(BLR) model a low-energy break/cutoff should be observed around photon energies  $\sim 4 (\Gamma/20)^2 \text{ keV}$ , while in the case of the EC(HDR) should be at around  $\sim 0.1 (\Gamma/20)^2 \text{ eV}$  (i.e., basically below the low-energy threshold of the available X-ray instruments). Noting however that the X-rays can be contributed by several other processes (such as SSC emission, bulk-Compton radiation, or high-energy emission of accretion disk corona), the apparent lack of the expected break can be used as an argument in favor of the EC(HDR) model only with caution.

## 8. HADRONS IN THE EC MODELS

If the EC models are correct, then the broadband blazar spectra allow us to estimate the number of jet electrons down to lowest energies, and to find the corresponding particle flux. However, since (by definition) in the “leptonic models” the entire observed radiative output of a jet is produced by primary (i.e., directly accelerated) electrons, the proton content of an outflow remains in principle unconstrained. The most recent analysis indicates that it cannot be negligible, though. In fact, several different authors came to the conclusion that the cold protons indeed dominate the jet bulk kinetic power, at least at  $> r_{\text{BLR}}$  scales, and that the number ratio of electron–proton to electron–positron pairs in quasar jets is of the order of 0.1–1 (Sikora & Madejski 2000; Celotti & Ghisellini 2008). Uncertainties regarding the proton content could be solved directly provided the acceleration of protons up to ultrarelativistic energies indeed takes place in the innermost parts of quasar jets

with high efficiency, and is followed by the production of some distinctive electromagnetic features, such as hardening of  $\gamma$ -ray spectra above 10 GeV or softening of X-ray spectra at lower energies. Again, lack of such spectral features does not exclude the dynamical role of protons in general, but only limits the number of ultrarelativistic hadrons, and thus constrains the particle acceleration models rather than the jet content.

In order to discuss this issue in more detail, we estimate the efficiency of the photo-meson production process for distances and magnetic fields appropriate for the EC models of luminous blazars. With the target photons provided by the local synchrotron emission of directly accelerated electrons, we have the appropriate opacity

$$\tau_{p\gamma}^{(\text{syn})}(\gamma_p) \simeq \langle \sigma_{p\gamma} K_{p\gamma} \rangle \frac{L_{\text{syn}} \gamma_p \zeta(\gamma_p)}{4\pi r \Gamma^3 m_\pi c^3}, \quad (73)$$

where  $\zeta(\gamma_p) < 1$  depends on the shape of the synchrotron spectrum (see Section 3.1). Assuming further that protons are injected with the same power-law index as directly accelerated jet electrons producing the observed  $\gamma$ -ray emission in the fast-cooling regime, we have  $s_p = 2\alpha_\gamma \geq 2$  for the typical  $\gamma$ -ray spectra of luminous blazars  $\alpha_\gamma \geq 1$  (Abdo et al. 2009b). Hence, because in addition  $\eta_{p\gamma}^{(\text{syn})}|_{s_p > 2} > \eta_{p\gamma}^{(\text{syn})}|_{s_p = 2}$  and  $\zeta(\gamma_p) < 1$ , we find using Equation (20) that

$$\eta_{p\gamma}^{(\text{syn})} < \langle \sigma_{p\gamma} K_{p\gamma} \rangle \frac{L_{\text{syn}}}{4\pi r \Gamma^3 m_\pi c^3} \frac{\gamma_{p,\text{max}}}{\ln \gamma_{p,\text{max}}} \quad (74)$$

which, for

$$\begin{aligned} \gamma_{p,\text{max}} &\simeq 5 \times 10^9 B'_G \left(\frac{f}{10}\right)^{-1} \left(\frac{r}{\text{pc}}\right) \left(\frac{\Gamma}{20}\right)^{-1} \\ &\simeq 3 \times 10^9 \left(\frac{f}{10}\right)^{-1} \left(\frac{L_B}{10^{46} \text{ erg s}^{-1}}\right) \left(\frac{\Gamma}{20}\right)^{-1} \end{aligned} \quad (75)$$

(see Section 3.1), gives finally

$$\begin{aligned} \eta_{p\gamma}^{(\text{syn})} &< 4 \times 10^{-4} \left(\frac{f}{10}\right)^{-1} \left(\frac{L_{\text{syn}}}{10^{47} \text{ erg s}^{-1}}\right) \left(\frac{L_B}{10^{46} \text{ erg s}^{-1}}\right)^{1/2} \\ &\times \left(\frac{\Gamma}{20}\right)^{-4} \left(\frac{r}{\text{pc}}\right)^{-1} \left(\frac{\ln \gamma_{p,\text{max}}}{24}\right)^{-1}. \end{aligned} \quad (76)$$

The particular value of the magnetic energy flux  $L_B \simeq 10^{46} \text{ erg s}^{-1}$  anticipated above is justified by Equations (38), (40), and (52), which in turn give

$$\frac{L_B}{L_{\text{disk}}} \simeq \left(\frac{\Gamma}{20}\right)^2 \left(\frac{q}{10}\right)^{-1} \times \begin{cases} 0.9 (\xi_{\text{BLR}}/0.1) \\ 0.5 (\xi_{\text{HDR}}/0.1) (T/10^3 \text{ K})^{2.6} \end{cases}. \quad (77)$$

As shown above, in the EC models for luminous blazars, high efficiency of the photo-meson production is expected only at distances  $r \ll 1 \text{ pc}$ . This implies that the maximal hadronic radiative output is reachable at around  $r \sim r_0$ , where the jet is already fully developed (i.e., accelerated and collimated), and the Doppler boosting is large. This efficiency can approach  $\sim (f/10)^{-1} (r_0/0.03 \text{ pc})^{-1} \%$ . Hence, even in this most optimistic case, the efficiency of the photo-meson production is much lower than the  $\sim 50\%$  radiative efficiency of jet electrons.

Let us further evaluate the number densities of the external (BLR and HDR) photon fields in the jet rest frame, approximating these by a monoenergetic distributions with the characteristic comoving photon energies  $h\nu'_{\text{BLR}} \simeq 200 (\Gamma/20) \text{ eV}$  and

$h\nu'_{\text{HDR}} \simeq 6 (\Gamma/20) \text{ eV}$ , respectively:

$$n'_{\text{BLR}} = \frac{u'_{\text{BLR}}}{h\nu'_{\text{BLR}}} \simeq 3 \times 10^{10} \left(\frac{\xi_{\text{BLR}}}{0.1}\right) \left(\frac{\Gamma}{20}\right) \quad (78)$$

at  $r_0 < r < r_{\text{BLR}}$  and

$$n'_{\text{HDR}} = \frac{u'_{\text{HDR}}}{h\nu'_{\text{HDR}}} \simeq 10^9 \left(\frac{T}{10^3 \text{ K}}\right)^{5.2} \left(\frac{\xi_{\text{HDR}}}{0.1}\right) \left(\frac{\Gamma}{20}\right) \quad (79)$$

at  $r_{\text{BLR}} < r < r_{\text{HDR}}$ . For  $\gamma_p > \gamma_{p,\text{th}}$ , where

$$\gamma_{p,\text{th}}^{(\text{BLR})} \simeq \frac{m_\pi c^2}{h\nu'_{\text{BLR}}} \simeq 7 \times 10^5 \left(\frac{\Gamma}{20}\right)^{-1} \quad (80)$$

and

$$\gamma_{p,\text{th}}^{(\text{HDR})} \simeq \frac{m_\pi c^2}{h\nu'_{\text{HDR}}} \simeq 2 \times 10^7 \left(\frac{\Gamma}{20}\right)^{-1}, \quad (81)$$

we have

$$\begin{aligned} \tau_{p\gamma}^{(\text{BLR})} &\simeq \langle \sigma_{p\gamma} K_{p\gamma} \rangle \frac{n'_{\text{BLR}} r}{\Gamma} \simeq 4 \times 10^{-2} \left(\frac{\xi_{\text{BLR}}}{0.1}\right) \left(\frac{r}{r_{\text{BLR}}}\right) \\ &\times \left(\frac{L_{\text{disk}}}{10^{46} \text{ erg s}^{-1}}\right)^{1/2} \end{aligned} \quad (82)$$

and

$$\begin{aligned} \tau_{p\gamma}^{(\text{HDR})} &\simeq \langle \sigma_{p\gamma} K_{p\gamma} \rangle \frac{n'_{\text{HDR}} r}{\Gamma} \simeq 4 \times 10^{-2} \left(\frac{\xi_{\text{HDR}}}{0.1}\right) \left(\frac{r}{r_{\text{HDR}}}\right) \\ &\times \left(\frac{L_{\text{disk}}}{10^{46} \text{ erg s}^{-1}}\right)^{1/2} \left(\frac{T}{10^3 \text{ K}}\right)^{2.6}. \end{aligned} \quad (83)$$

Hence, this implies the total photo-meson production efficiency to be

$$\begin{aligned} \eta_{p\gamma}^{(\text{BLR})} &\leq 4 \times 10^{-2} \left(\frac{\xi_{\text{BLR}}}{0.1}\right) \left(\frac{r}{r_{\text{BLR}}}\right) \left(\frac{L_{\text{disk}}}{10^{46} \text{ erg s}^{-1}}\right)^{1/2} \\ &\times \frac{\ln(\gamma_{p,\text{max}}/\gamma_{p,\text{th}}^{(\text{BLR})})}{\ln \gamma_{p,\text{max}}} \end{aligned} \quad (84)$$

for  $r_0 < r < r_{\text{BLR}}$  and

$$\begin{aligned} \eta_{p\gamma}^{(\text{HDR})} &\leq 4 \times 10^{-2} \left(\frac{\xi_{\text{HDR}}}{0.1}\right) \left(\frac{r}{r_{\text{HDR}}}\right) \left(\frac{L_{\text{disk}}}{10^{46} \text{ erg s}^{-1}}\right)^{1/2} \\ &\times \left(\frac{T}{10^3 \text{ K}}\right)^{2.6} \frac{\ln(\gamma_{p,\text{max}}/\gamma_{p,\text{th}}^{(\text{HDR})})}{\ln \gamma_{p,\text{max}}} \end{aligned} \quad (85)$$

for  $r_{\text{BLR}} < r < r_{\text{HDR}}$ . Note that the calculated efficiencies never exceed  $\sim 1\%$ .

Summarizing this section, we conclude that some imprints of hadronic activity in the EC-dominated high-energy blazar spectra are anticipated only if the blazar zone is located at  $r_0 < r < r_{\text{BLR}}$ . Still, this would require almost unrealistically efficient proton acceleration, with  $f < 10$ . Any hadronic activity is expected to be completely absent in the blazar spectra if the blazar emission zone is located at distances  $r > r_{\text{BLR}}$  (i.e., at distances where the EC(HDR) process dominates), or if  $f > 10$ .

## 9. DISCUSSION

According to the analysis presented in the previous sections, the broadband emission of luminous blazars cannot be easily explained in the framework of the hadronic scenarios or the SSC model, but instead is consistent with the EC models. In addition, the EC(HDR) model is favored over the EC(BLR) variant. This, in turn, fixes the location of the blazar emission zone at  $r \sim 1\text{--}10$  pc from the nucleus. Note that in the EC(BLR) model, the high-energy blazar emission is produced deeply within the millimeter photosphere and therefore one should not expect simultaneous high-amplitude  $\gamma$ -ray and mm-band variability. In contrast, in the EC(HDR) model the blazar zone extends up to the millimeter photosphere, and thus mm-band variations accompanying  $\gamma$ -ray flares are expected, as in fact observed, e.g., during the 2006 outburst event in 3C 454.3 (Krichbaum et al. 2008). Hence, systematic monitoring of luminous blazars at mm/sub-mm wavelengths and GeV photon energies is of primary interest, allowing us to confirm our conclusions.

Regardless of the observational verification, advocating the EC(HDR) model requires addressing the following questions: (1) Why is the blazar emission zone located at some particular (and, quite large:  $r \sim 10^5 R_g$  for  $10^9 M_\odot$  black hole!) distance from the nucleus? (2) What is the dominant particle acceleration process involved, and why is it restricted to the relatively narrow distance range along the outflow? These questions are in fact related, since the location of the blazar emission zone is primarily determined by the energy dissipation processes rather than by some other factors, such as the presence of seed photons for IC scattering, i.e., the enhanced radiative cooling of jet electrons. To justify this statement, in Figure 3 we have plotted energy densities of different photon fields (and also of the jet magnetic field), all as measured in the jet rest frame, as functions of the distance from the center  $r$ . Here we assumed a fully developed outflow with the main parameters corresponding to the analysis presented in the previous sections. As shown, the total energy density of different fields contributing to radiative cooling of jet particles,  $u'_{\text{tot}} = u'_B + u'_{\text{BLR}} + u'_{\text{HDR}} + \dots$ , decreases along the jet roughly as  $u'_{\text{tot}} \propto r^{-2}$ , being initially dominated by the magnetic field energy density ( $r \lesssim 0.03$  pc), later by the energy density of the BLR ( $r \sim 0.03\text{--}1$  pc), and next by the energy density of the HDR ( $r \gtrsim 1$  pc). Thus, no particular distance scale is favored as long as solely the  $u'_{\text{tot}}$  parameter is considered.

The location of the blazar emission zone must be then determined by the energy dissipation/particle acceleration processes within relativistic outflow, responsible for the generation of the non-thermal electron population. In general (though most likely also quite naively), one can expect that the dominant acceleration mechanism should be related to the magnetic reconnection process in the case of a jet dominated by the magnetic field, and to the Fermi-type processes in the case of a matter-dominated outflow. In this context, we note that the most recent models for the jet formation indicate that AGN jets are in fact dominated by the Poynting flux (and are stable against current-driven Z-pinch instabilities) up to at least  $r \sim 10^3 R_g$  (see, e.g., McKinney & Blandford 2009 and references therein). At further distances from the jet base, AGN outflows may be considered as fully developed (i.e., accelerated and collimated to the terminal values of  $\Gamma$  and  $\theta_j$  parameters), and likely (though not necessarily) converted to matter-dominated structures due to the development of various (mainly kink and pinch) current-driven instabilities. Such instabilities provide a sink for the jet magnetic field, and

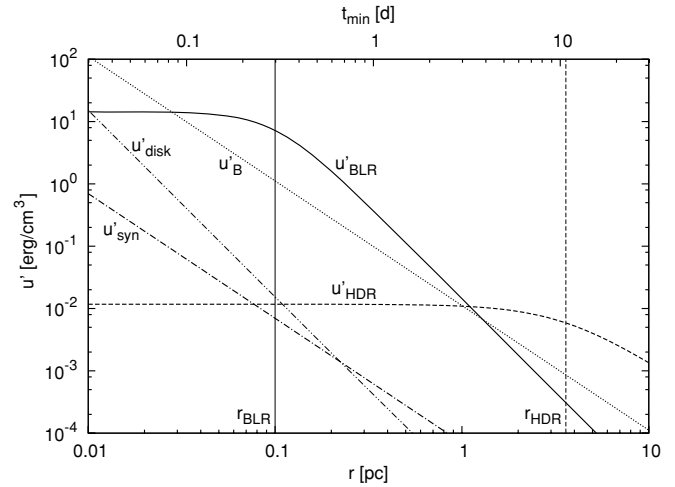


**Figure 3.** Energy densities of broad-line emission (solid line), hot dust radiation (dashed line), magnetic field (dotted line), synchrotron radiation (dot-dashed line), and accretion disk emission (thin double-dot-dashed line) as seen in the jet comoving frame, as a function of distance from the central engine. The shortest timescale of flares corresponding to the jet radius  $R = r/\Gamma$  at a given distance from the center  $r$ , as measured in the observer frame, is shown on the top axis. The characteristic radii of broad-line region  $r_{\text{BLR}}$  and dusty torus  $r_{\text{HDR}}$  are indicated with a solid and a dashed vertical line, respectively. We assumed here jet bulk Lorentz factor  $\Gamma = 20$ , accretion disk luminosity  $L_{\text{disk}} = 10^{46}$  erg s $^{-1}$ , synchrotron luminosity  $L_{\text{syn}} = 10^{47}$  erg s $^{-1}$ , magnetic flux  $L_B = 10^{46}$  erg s $^{-1}$ , broad-line region covering factor  $\xi_{\text{BLR}} = 0.1$ , dusty torus covering factor  $\xi_{\text{HDR}} = 0.1$ , and dust temperature  $T_{\text{dust}} = 10^3$  K. We assume that beyond  $r_{\text{BLR}}$  stratification of the broad-line emission takes form  $dL_{\text{BLR}}/d \ln r \propto 1/r$ , and hence  $u'_{\text{BLR}} \propto r^{-3}$  for  $r > r_{\text{BLR}}$ . Radiation energy density from the accretion disk is calculated using the formula  $u'_d \simeq 0.28 (L_{\text{disk}}/4\pi r^2 c) (R_g/r)\Gamma^2$  for  $R_g$  of the fast-rotating black hole with mass  $M_{\text{BH}} = 10^9 M_\odot$  (Dermer & Schlickeiser 2002).

energize jet particles by forming shocks within, and/or injecting turbulence into the outflow.

Not much is known about the magnetic reconnection in the relativistic regime; in particular, the accompanying particle acceleration processes remain elusive (see Lyubarsky 2005; Lyubarsky & Liverts 2008; Lyutikov & Uzdensky 2003). The results of the analysis presented in this paper, which suggest that the bulk of the blazar emission is produced far away from the jet base, may thus be taken as an indication for a low efficiency of the electron acceleration within the innermost, magnetically dominated parts of quasar jets. That is to say, the reconnection-driven acceleration processes may still operate at distances  $r < 10^3 R_g$ , but the resulting radiative output does not seem to be sufficiently strong to dominate over the emission produced further out from the nuclei of such luminous blazars. In other words, the efficiency of particle acceleration has to increase significantly at some larger distance from the core. And indeed, as mentioned above, initially suppressed current-driven instabilities are supposed to develop starting from  $r \sim 10^3 R_g$ , i.e.,  $r \sim 0.03$  pc for a  $10^9 M_\odot$  black hole, where the BLR dominates the radiative cooling of the jet electrons. Still, this is about two orders of magnitude below the location of a blazar emission zone favored by our analysis.

One can propose some ad hoc explanation for the apparent discrepancy indicated above, such as, for example, the stabilizing role of a velocity shear within relativistic outflow (cf. Mizuno et al. 2007), precluding formation of shocks or strong turbulence up to the distances of  $\sim 10^4 R_g$  and beyond. The other possible explanation would be to postulate that the energy dissipation processes associated with the internal shocks

formed due to steepening of kink instabilities around  $10^3 R_g$  are much less efficient in accelerating jet electrons to ultrarelativistic energies than the analogous mechanism associated with, e.g., extended reconfinement shocks formed further out from the nucleus. In fact, a role of reconfinement shocks in shaping radiative and morphological properties of blazar jets has been discussed previously by several authors (Jorstad et al. 2001a, 2001b; Cheung et al. 2007; Sikora et al. 2008; Nalewajko & Sikora 2009; Bromberg & Levinson 2009). The reason for such a difference in the acceleration efficiency may be due to the different turbulence/magnetic field conditions for both kink-driven and reconfinement shocks: note that the most recent analysis of the shock acceleration in a relativistic regime clearly shows the importance of background (plasma) conditions around the shock front in shaping the spectral properties of non-thermal particles generated there (e.g., Niemiec & Ostrowski 2004; Sironi & Spitkovsky 2009).

But should the dominant particle acceleration process in quasar jets be undoubtedly identified with shocks? In fact, there are strong indications for this. Note, first, that the maximum energy of ultrarelativistic electrons responsible for the electromagnetic emission of luminous blazars is not high ( $\gamma \lesssim 10^4$ ). Meanwhile, by equating the radiative cooling timescale  $t'_{\text{cool}} \sim m_e c / \sigma_T \gamma u'_{\text{tot}}$  with the electron acceleration timescale  $t'_{\text{acc}} \sim f \gamma m_e c / e B'$ , one gets the maximum available electron energy  $\gamma \sim 10^4$  for the acceleration efficiency parameter as low as  $f^{-1} \sim 10^{-7} - 10^{-8}$  at any distance  $0.01 \text{ pc} \lesssim r \lesssim 10 \text{ pc}$ . In other words, the maximum electron energy, if limited solely by the radiative energy losses, might be expected to be much higher than that observed, since the often invoked “maximum” efficiency of particle acceleration in a cosmic plasma corresponds to  $f^{-1} \sim 0.1$  (see also in this context Inoue & Takahara 1996). Second, the electron energy distribution reconstructed from the observed broadband electromagnetic spectra of luminous blazars seems to be best approximated by a broken power law,  $N_\gamma \propto \gamma^{-s}$  with  $s \leq 2$  for  $\gamma < \gamma_{\text{cr}} \lesssim 10^3$ , and  $s > 2$  for  $\gamma > \gamma_{\text{cr}}$ . This manifests itself in the so-called blazar sequence (Fossati et al. 1998), which, even though it is still pending the observational confirmation, reflects the robust finding that the peak electron energy in powerful, quasar-hosted blazars is always  $\gamma_{\text{cr}} \lesssim 10^3$  (see Celotti & Ghisellini 2008). In fact, exactly this kind of electron spectrum is expected to form at relativistic (perpendicular) shock mediated by cold protons, for which the proton inertia (and not the radiative cooling rate!) determines the critical electron energy  $\gamma_{\text{cr}} \lesssim m_p / m_e \sim 10^3$ , as discussed in Stawarz et al. (2007) for the case of terminal shocks in quasar jets.

In other words, the electron energy distribution “reconstructed” from the broadband emission spectra of luminous blazars indicates that the appropriate acceleration processes are related to relativistic shocks formed in a matter (proton)-dominated outflow. This assures self-consistency of the EC models favored by our analysis. We note in this context, that the low-energy segment of the electron energy distribution discussed above ( $\gamma < \gamma_{\text{cr}}$ ) is expected to form not due to the diffusive (first-order Fermi) shock acceleration (which may operate only at  $\gamma > \gamma_{\text{cr}}$ ), but due to interactions of relativistic electrons (with gyroradii smaller than Larmor radii of cold protons) with turbulence and electromagnetic waves *within* the shock front. The best studied process of this type is a resonant absorption of proton cyclotron emission (produced by cold hadrons reflected from a magnetized perpendicular shock front) by the jet electrons, as discussed first by Hoshino et al. (1992). Interestingly,

the most recent analysis of this mechanism (Amato & Arons 2006) reveals a power-law form of the electron energy distribution  $N_\gamma \propto \gamma^{-s}$  with  $1 < s \lesssim 2$  (depending on the plasma composition) within the electron energy range  $1 < \gamma < \Gamma_{\text{sh}} m_p / m_e$ , where  $\Gamma_{\text{sh}}$  is the shock bulk Lorentz factor in the upstream plasma rest frame. This is in fact in a very good agreement with the hard X-ray spectra observed in luminous blazars, which in turn often exhibit X-ray spectral indices  $\alpha_x < 0.5$  (see Table 1), and with the general form of the electron spectrum invoked in modeling blazar spectra (Celotti & Ghisellini 2008; Ghisellini & Tavecchio 2008).

## 10. CONCLUSIONS

1. Hadronic models cannot reproduce the very hard X-ray spectra observed in a number of luminous blazars; they also require extremely (almost unrealistically) efficient acceleration of relativistic protons to the highest energies within the inner parts of the outflow, and the jet kinetic power exceeding the Eddington luminosity by orders of magnitude.
2. The SSC model, which can account for the hard X-ray spectra and also for the synchrotron and IC peak frequencies observed in luminous blazars, requires significant departures from the minimum power condition in order to explain large luminosity ratio of the low- and high-energy spectral components; furthermore, in a dense radiative environment of quasar nuclei, energy density of the external radiation fields (provided inevitably by BLR and HDR) strongly dominates (in a jet rest frame) over the energy density of the internal jet synchrotron photons, and therefore the EC emission is expected to dominate over the SSC emission.
3. The EC models—both EC(BLR) and EC(HDR) variants—can easily account for the large- $q$  states of luminous blazars, their hard X-ray spectra, and the observed ratio of synchrotron and IC peak frequencies; in addition, the main jet parameters implied by these models (such as  $\Gamma$ ,  $L_j$ , etc.) are consistent with a number of different observational constraints.
4. Lack of the bulk-Compton and the KN features in the broadband spectra of luminous blazars, as well as the absence of the low-energy cutoff in their X-ray continua, seems to favor the EC(HDR) model over the EC(BLR) variant; however, these particular constraints have to be taken with caution, and are not definitive as yet.
5. The most promising observational discrimination between the EC(BLR) and EC(HDR) models may be provided by confirmation of the characteristic variability timescale of luminous blazars being days/weeks, and by the detection of high-amplitude variability in mm-band systematically accompanying  $\gamma$ -ray flares. The previous observational results seem to be in fact in agreement with the predictions of the EC(HDR) model; more high-quality, well-sampled data are however needed in this context, and these are expected to be provided in a near future by recently launched *Fermi Gamma-ray Space Telescope* surveying the whole sky, in conjunction with well-sampled multi-band observing campaigns.
6. The electron energy distribution “reconstructed” from the broadband emission spectra of luminous blazars indicates that the appropriate acceleration processes are related to relativistic shocks formed in a proton-dominated outflow. This assures self-consistency of the favored EC models, in

which the blazar emission zone is located far away from the nucleus ( $r > 10^3 R_g$ ), where the jet may be considered as already fully formed (i.e., accelerated and collimated), and converted to a matter-dominated structure.

We acknowledge financial support by NASA grants NNX08AZ77G and NNX09AG12G, by the Department of Energy contract to SLAC No. DE-AE3-76SF00515, by the Polish MNiSW grant N N203 301635, N N203 380336, and the Polish Astroparticle Network 621/E-78/BWSN-0068/2008.

## REFERENCES

- Abdo, A. A., et al. 2009a, *ApJ*, 697, 934  
 Abdo, A. A., et al. 2009b, *ApJS*, 183, 46  
 Aharonian, F. A. 2000, *New Astron.*, 5, 377  
 Aharonian, F. A., et al. 2002, *Phys. Rev. D*, 66, 023005  
 Amato, E., & Arons, J. 2006, *ApJ*, 653, 325  
 Barvainis, R. 1987, *ApJ*, 320, 537  
 Begelman, M. C., Rudak, B., & Sikora, M. 1990, *ApJ*, 362, 38  
 Begelman, M. C., & Sikora, M. 1987, *ApJ*, 322, 650  
 Bonning, E. W., et al. 2009, *ApJ*, 697, L81  
 Böttcher, M. 2007, *Ap&SS*, 309, 95  
 Bromberg, O., & Levinson, A. 2009, *ApJ*, 699, 1274  
 Celotti, A., & Ghisellini, G. 2008, *MNRAS*, 385, 283  
 Celotti, A., Ghisellini, G., & Fabian, A. C. 2007, *MNRAS*, 375, 417  
 Cheung, C. C., Harris, D. E., & Stawarz, L. 2007, *ApJ*, 663, L65  
 Cleary, K., Lawrence, C. R., Marshall, J. A., Hao, L., & Meier, D. 2007, *ApJ*, 660, 117  
 Collmar, W., et al. 2007, in Proc. of the *VINTEGRAL* Workshop, The Obscured Universe, ed. S. Grebenev, R. Sunyaev, & C. Winkler (Noordwijk: ESA), 207  
 Dermer, C. D. 1995, *ApJ*, 446, 63  
 Dermer, C. D., & Atoyan, A. M. 2002, *ApJ*, 568, L81  
 Dermer, C. D., & Schlickeiser, R. 2002, *ApJ*, 575, 667  
 De Rosa, A., Bassani, L., Ubertini, P., Malizia, A., & Dean, A. J. 2008, *MNRAS*, 388, L54  
 De Rosa, A., et al. 2005, *A&A*, 438, 121  
 Donato, D., Sambruna, R. M., & Gliozzi, M. 2005, *A&A*, 433, 1163  
 Fabian, A. C., et al. 1998, *MNRAS*, 295, L25  
 Fossati, G., et al. 1998, *MNRAS*, 299, 433  
 Gear, W. K., et al. 1994, *MNRAS*, 267, 167  
 Ghisellini, G., & Tavecchio, F. 2008, *MNRAS*, 387, 1669  
 Giommi, P., et al. 2002, in ASI Science Data Center, ESA-ESRIN, Blazar Astrophysics with BeppoSAX and Other Observatories, ed. P. Giommi, E. Massaro, & G. Palumbo (Frascati, Italy: ESA-ESRIN), 63  
 Giommi, P., et al. 2007, *A&A*, 468, 571  
 Glikman, E., Helfand, D. J., & White, R. L. 2006, *ApJ*, 640, 579  
 Hartman, R. C., et al. 1999, *ApJS*, 123, 79  
 Hoshino, M., Arons, J., Gallant, Y. A., & Langdon, A. B. 1992, *ApJ*, 390, 454  
 Inoue, S., & Takahara, F. 1996, *ApJ*, 463, 555  
 Jorstad, S. G., et al. 2001a, *ApJ*, 556, 738  
 Jorstad, S. G., et al. 2001b, *ApJS*, 134, 181  
 Kataoka, J., et al. 2008, *ApJ*, 672, 787  
 Komissarov, S. S., Barkov, M. V., Vlahakis, N., & Königl, A. 2007, *MNRAS*, 380, 51  
 Kovalev, Y. Y., et al. 2009, *ApJ*, 696, L17  
 Krichbaum, T. P., et al. 2008, in ASP Conf. Ser. 386, Extragalactic Jets: Theory and Observation from Radio to Gamma Ray, ed. T. A. Rector & D. S. De Young (San Francisco, CA: ASP), 186  
 Labita, M., Treves, A., & Falomo, R. 2008, *MNRAS*, 383, 1513  
 Lawson, A. J., & McHardy, I. M. 1998, *MNRAS*, 300, 1023  
 Levinson, A. 2006, *Int. J. Mod. Phys. A*, 21, 6015  
 Lister, M. L., et al. 2009, *ApJ*, 696, L22  
 Lyubarsky, Y. E. 2005, *MNRAS*, 358, 113  
 Lyubarsky, Y. E., & Liverts, M. 2008, *ApJ*, 682, 1436  
 Lyutikov, M., & Uzdensky, D. 2003, *ApJ*, 589, 893  
 Mannheim, K. 1993, *A&A*, 269, 67  
 Mannheim, K., & Biermann, P. L. 1992, *A&A*, 253, L21  
 Marshall, H. L., et al. 2005, *ApJS*, 156, 13  
 McKinney, J. C., & Blandford, R. D. 2009, *MNRAS*, 394, L126  
 Mizuno, Y., Hardee, P., & Nishikawa, K. I. 2007, *ApJ*, 662, 835  
 Moderski, R., Sikora, M., & Błażejowski, M. 2003, *A&A*, 406, 855  
 Moderski, R., Sikora, M., Coppi, P. S., & Aharonian, F. 2005, *MNRAS*, 364, 1488  
 Moderski, R., Sikora, M., Madejski, G. M., & Kamae, T. 2004, *ApJ*, 611, 770  
 Nalewajko, K., & Sikora, M. 2009, *MNRAS*, 392, 1205  
 Nenkova, M., et al. 2008, *ApJ*, 685, 156  
 Netzer, H., et al. 2007, *ApJ*, 666, 806  
 Niemiec, J., & Ostrowski, M. 2004, *ApJ*, 610, 851  
 Pica, A. J., et al. 1988, *AJ*, 96, 1215  
 Raiteri, C. M., et al. 2008, *A&A*, 485, L17  
 Reeves, J. N., et al. 2001, *A&A*, 365, L134  
 Reimer, A., Protheroe, R. J., & Donea, A.-C. 2004, *A&A*, 419, 89  
 Sambruna, R. M., et al. 2007, *ApJ*, 669, 884  
 Siemiginowska, A., et al. 2008, *ApJ*, 684, 811  
 Sikora, M., Begelman, M. C., Madejski, G. M., & Lasota, J.-P. 2005, *ApJ*, 625, 72  
 Sikora, M., & Madejski, G. M. 2000, *ApJ*, 534, 109  
 Sikora, M., & Madejski, G. M. 2001, in ASP Conf. Ser. 558, High Energy Gamma-Ray Astronomy: International Symposium, ed. F. A. Aharonian & H. J. Volk (San Francisco, CA: ASP), 275  
 Sikora, M., Madejski, G. M., Moderski, R., & Poutanen, J. 1997, *ApJ*, 484, 108  
 Sikora, M., Moderski, R., & Madejski, G. M. 2008, *ApJ*, 675, 71  
 Sironi, L., & Spitkovsky, A. 2009, *ApJ*, 698, 1523  
 Spada, M., Ghisellini, G., Lazzati, D., & Celotti, A. 2001, *MNRAS*, 325, 1559  
 Stawarz, L., Cheung, C. C., Harris, D. E., & Ostrowski, M. 2007, *ApJ*, 662, 213  
 Tavecchio, F., & Ghisellini, G. 2008, *MNRAS*, 386, 945  
 Watanabe, S., et al. 2009, *ApJ*, 694, 294  
 Worsley, M. A., Fabian, A. C., Celotti, A., & Iwasawa, K. 2004, *MNRAS*, 350, L67